

# Local spectroscopy of the Kondo lattice $\text{YbAl}_3$ : Seeing beyond the surface with scanning tunneling microscopy and spectroscopy

P. Wahl,<sup>1</sup> L. Diekhöner,<sup>1,\*</sup> M. A. Schneider,<sup>1,†</sup> F. Treubel,<sup>2,‡</sup> C. T. Lin,<sup>1</sup> and K. Kern<sup>1,3</sup>

<sup>1</sup>Max-Planck-Institut für Festkörperforschung, Heisenbergstr. 1, D-70569 Stuttgart, Germany

<sup>2</sup>Department of Physics, Universität Konstanz, D-78457 Konstanz, Germany

<sup>3</sup>Institut de Physique de la Matière Condensée, Ecole Polytechnique Fédérale de Lausanne (EPFL), CH-1015 Lausanne, Switzerland

(Received 30 September 2011; revised manuscript received 14 November 2011; published 27 December 2011)

We report on an atomic-scale study of the Kondo lattice compound  $\text{YbAl}_3$  using scanning tunneling microscopy (STM) and spectroscopy (STS). An analysis of the surface orientation and structure is performed based on STM images containing more than one crystal facet. We compare tunneling spectra acquired on different facets and discuss their relation with the temperature scales observed in measurements of bulk quantities and the states observed in photoemission spectra. On specific facets, we observe strong additional resonances close to the Fermi energy which are not consistent with the characteristic energy scales found in bulk measurements, and which we interpret in terms of a modified Kondo state of the near-surface Ytterbium atoms.

DOI: [10.1103/PhysRevB.84.245131](https://doi.org/10.1103/PhysRevB.84.245131)

PACS number(s): 72.10.Fk, 68.37.Ef, 72.15.Qm

## I. INTRODUCTION

Correlated electron materials exhibit pronounced anomalies in their macroscopic properties which are yet poorly understood. An important piece of the puzzle is a precise knowledge of the electronic structure in the vicinity of the Fermi energy. A measurement of the local density of states (LDOS) close to the Fermi energy provides a benchmark for theories<sup>1,2</sup> and might offer insight into the origin of the anomalies in the macroscopic properties of these materials. An obstacle to studying their electronic structure with angular resolved photoemission (ARPES) or scanning tunneling spectroscopy (STS) is the often unclear relation between surface and bulk properties. At the same time, the broken translational symmetry and the reduced dimensionality as found at the surface can lead to interesting new phenomena.<sup>3–5</sup> While for Ce and U compounds the surface influence appears to be negligible,<sup>6–8</sup> this is different for Yb compounds as indicated by studies with x-ray photoemission spectroscopy and ARPES.<sup>5,9,10</sup> In photoemission studies, the valence of ytterbium in the near surface region is found to deviate from the valence of ytterbium in the bulk. However, previous studies of the surface of  $\text{YbAl}_3$  have been performed with techniques averaging over extended surface areas,<sup>9,10</sup> therefore being unable to disentangle the influence of the surface orientation and defects. Only recently, scanning tunneling microscopy and spectroscopy has been applied to another ytterbium compound  $\text{YbRh}_2\text{Si}_2$ , revealing a set of resonances close to the Fermi energy consistent with excitations observed in neutron scattering.<sup>11</sup>

We have studied an ytterbium-based Kondo lattice compound  $\text{YbAl}_3$  by scanning tunneling microscopy (STM) and STS to address this issue.  $\text{YbAl}_3$  is well characterized by bulk methods, thus allowing us to relate features in the tunneling spectra to bulk properties. Magnetization measurements of  $\text{YbAl}_3$  reveal a clear deviation from a Curie law behavior.<sup>12</sup> The temperature dependence of the magnetic susceptibility exhibits two maxima, one at  $\sim 130$  K and one at  $\sim 20$  K. The maximum at  $\sim 130$  K has been rationalized by a screening of the spins of the ytterbium atoms by the conduction electrons, hence by the Kondo effect. The low temperature maximum

has been attributed to a crossover to a coherent Kondo lattice state below 40 K.<sup>13–15</sup> The reported characteristic Kondo temperature of the system varies between 225 and 670 K depending on the method by which it is obtained.<sup>13,16,17</sup>

Several photoemission studies<sup>18,19</sup> have been performed on  $\text{YbAl}_3$  with the aim of detecting the Kondo resonance, the spectral signature of the Kondo effect. Photoemission spectra of  $\text{YbAl}_3$  expose a distinct peak within 300 meV below the Fermi energy.<sup>17–20</sup> One of the difficulties in comparing the various photoemission measurements is that spectra are obtained from crystals of strongly differing quality, ranging from *in situ* grown polycrystalline samples,<sup>18</sup> *in situ* fractured polycrystalline samples,<sup>19</sup> and flux-grown single crystals cleaved in ultrahigh vacuum (UHV)<sup>20</sup> to *in situ* scraped polycrystalline samples.<sup>17</sup> Besides an unknown quality of the surface, photoemission likely averages over multiple facets or even several crystallites. In order to relate measurements of surface sensitive probes like STM or photoemission to bulk properties, a careful assessment of the influence of the surface is required. Photoelectron spectroscopy of both ytterbium aluminum bulk alloys and ytterbium deposited on an aluminum single crystal surface has shown that ytterbium ions become divalent at the surface, while their mixed valence character as found in the bulk recovers within  $\approx 5$  Å of the surface.<sup>9,10</sup>

## II. EXPERIMENTAL METHODS

The  $\text{YbAl}_3$  samples used for our experiments have been grown using the Czochralski pulling method. STM and SQUID measurements have been performed on slices of  $\sim 2$  mm thickness and a diameter of  $\sim 5$  mm cut from the crystals. The samples were polycrystalline, and scanning electron microscopy shows that the size of the grains is about 500  $\mu\text{m}$  in diameter with regions of up to 20  $\mu\text{m}$  of undefined composition in between. Thus individual grains are significantly larger than the length scales on the order of 10 to 100 nm probed by STM. STM measurements have been performed on two samples, which have been oriented by x-ray diffraction such that crystallites are oriented predominantly in the (110) direction. Since the samples are polycrystalline,

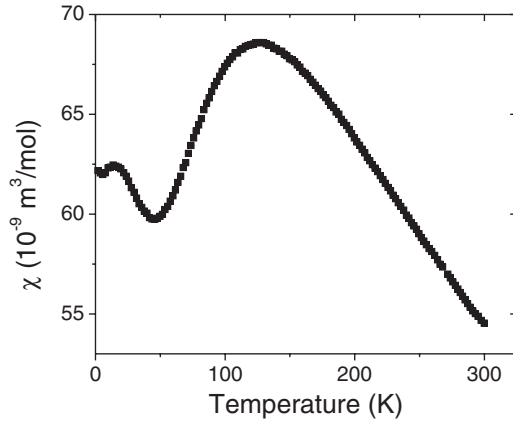


FIG. 1. SQUID magnetization measurements on a bulk  $\text{YbAl}_3$  sample. The temperature dependence exhibits two maxima: one at 126 K which corresponds to the energy scale of single impurity screening, and one at 16 K which may be related to the onset of coherence.

the grains have random orientations and the (110) direction will at best dominate. The surfaces of both samples have been polished. After transfer to UHV, the surface has been treated by sputtering and annealing cycles to remove surface contaminations. During the first cycles, the sample was heated to 700 K; in later sputtering cycles we annealed only to 600–650 K. STM measurements have been performed in a home-built low temperature UHV-STM which operates at temperatures down to 6.7 K. In this paper, measurements

performed at 6.7 and 77 K are shown. Tunneling spectra have been acquired with an open feedback loop recording the  $dI/dV$  signal from a lock-in amplifier; bias voltages are applied to the sample with the tip at virtual ground.

### III. RESULTS

#### A. Bulk characterization

After preparation of the samples, we have characterized the bulk properties by SQUID measurements (Fig. 1). The temperature dependence of the magnetic susceptibility is consistent with earlier work.<sup>21,22</sup> From the zero temperature limit of the magnetic susceptibility as extracted from the SQUID measurements, the Kondo temperature can be extracted if the number of holes in the  $f$  orbital  $n_f = v - 2$  of the magnetic ions is known (where  $v$  is the valence of the ions).<sup>19,23</sup> We obtain for the Kondo temperature with  $\chi(0) = 6.2 \cdot 10^{-8} \frac{\text{m}^3}{\text{mol}}$

$$\frac{T_K}{n_f} = \frac{1}{3} \frac{\mu_0 \mu_{\text{eff}}^2}{k_B \chi(0)} \approx 521 \text{ K.} \quad (1)$$

The valence  $v$  has been determined previously from photoemission spectra yielding values between 2.6<sup>17,24</sup> and 2.8<sup>19</sup> and from x-ray absorption giving 2.75–2.77 at 4 K.<sup>13,17</sup> Here we use  $v = 2.7 \pm 0.1$  resulting in a Kondo temperature  $T_K \approx 365 \pm 52 \text{ K}$ .

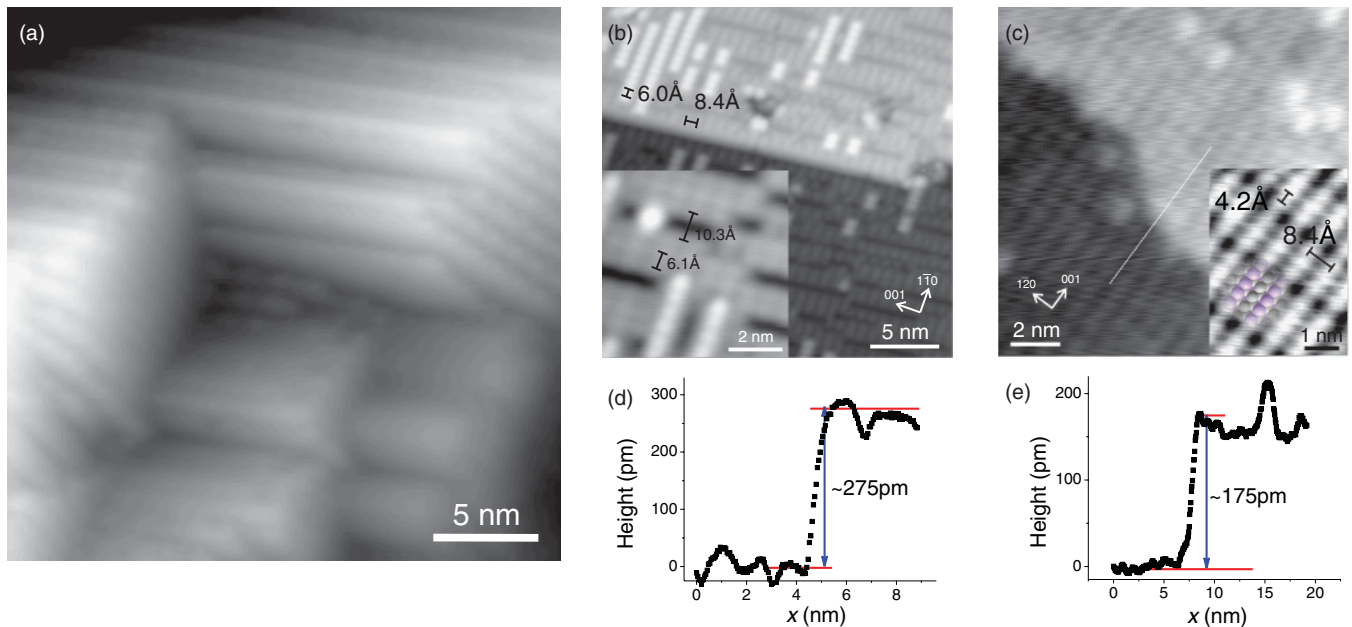


FIG. 2. (Color) (a) Overview topography obtained on the surface of the  $\text{YbAl}_3$  sample after preparation as described in the main text ( $26 \times 26 \text{ nm}^2$ ). Different crystallographic facets are observed ( $V = 0.35 \text{ V}$ ,  $I = 3 \text{ nA}$ ). (b) image of a (110) facet ( $V = -0.9 \text{ V}$ ,  $I = 1.4 \text{ nA}$ ), (c) image of a (210) facet ( $V = 0.1 \text{ V}$ ,  $I = 1.4 \text{ nA}$ ). The dashed line drawn on top of the bright lines on the upper terrace shows that the lines on the upper terrace are shifted with respect to those of the lower terrace as expected for a (210) facet. Insets in (b) and (c) show zoomed-in topographies of the facets; for the (210) facet [in (c)] a simple ball model of the surface is also shown. (The model can be drawn on top of the topography in two equivalent ways, only one of them is shown; the atoms shown in light gray correspond to Al atoms, the ones in purple to Yb atoms.) Tunneling parameters for the insets: (b)  $V = 1.8 \text{ V}$ ,  $I = 3 \text{ nA}$ , (c)  $V = 0.5 \text{ V}$ ,  $I = 3 \text{ nA}$ . (d) and (e) Line cuts across a step edge on a (110) and (210) facet, respectively.

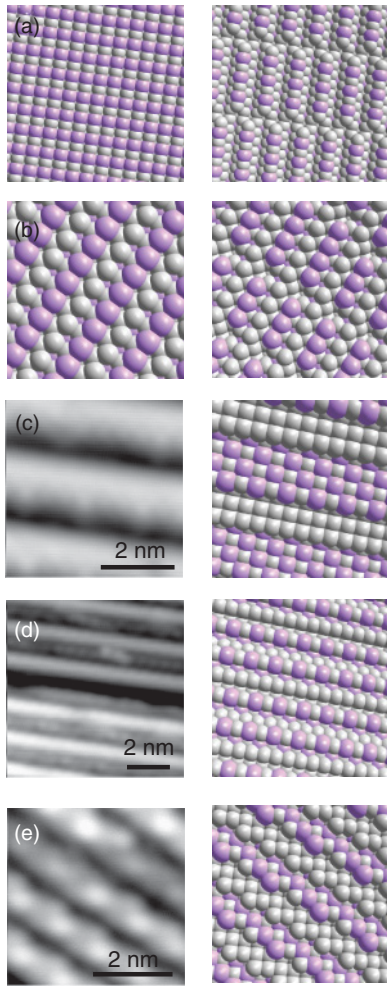


FIG. 3. (Color) (a) and (b) Model of the (110) and (210) facets without reconstruction (left) and with a proposed model for the reconstruction (right); atomically resolved STM topographies of the same surfaces can be seen in Figs. 2(b) and 2(c). (c)–(e) Closeups of the facets considered. Shown are topographies and ball models for (c) a (611) facet ( $V = 0.346$  V,  $I = 3$  nA), (d) a (522) facet ( $V = 0.349$  V,  $I = 3$  nA), and (e) a (931) facet ( $V = -22$  mV,  $I = 0.31$  nA). Ytterbium atoms are shown as purple balls, aluminum atoms as gray balls.

**B. Topographic Images**

In STM, we find the surface typically as shown in Fig. 2(a): sometimes exposing facets with different crystallographic orientations within one topographic image, occasionally also large areas exposing only a single facet. The facets exposed within an area on the order of  $(25 \text{ nm})^2$  can be assumed to belong to a single crystallite. Thus by investigating the surface structure of different facets as seen in Fig. 2(a), we can ensure that the crystal structure of the crystallite is at least in the surface region (apart from possible reconstruction) consistent with that of  $\text{YbAl}_3$ . We have determined the Miller indices of the facets in two ways: The first route we used is to determine the periodicity of the exposed facet by measuring lateral interatomic distances in the topographic image [see, e.g., Figs. 2(b) and 2(c)]. The inset of Fig. 2(b) shows a closeup of a (110) facet and that of Fig. 2(c) of a (210) facet revealing the atomic scale structure. Both facets show a reconstruction

of the surface layer. Due to the much larger ionic radius of ytterbium compared to aluminum, we speculate that ytterbium atoms are imaged as higher protrusions. With this assumption, in the case of the (210) facet every 3rd or 4th ytterbium atom along the close-packed rows is missing. The (110) facet is more strongly reconstructed with every second row of atoms missing.

The extracted length scales can be compared to the ideal surface structure neglecting relaxation and reconstruction. This works well for low index facets, however it becomes more ambiguous the larger the Miller indices are, because facets with different indices can have comparable periodicities. As an additional test for the assignment of the Miller indices, step edges can be used if they are observed. We found step edges for the two low index facets (110) and (210) [see Figs. 2(b) and 2(c), line cuts are shown in Figs. 2(d) and 2(e)], so that the step height and the structure of adjacent terraces can be compared to the surface structure extracted from the crystal structure. Representative STM topographies and ball models for the other facets which we have observed are shown in Fig. 3.

The second method uses the relative orientation of the facets in STM topographies where more than one facet is found in a single STM topography, as can be seen in Fig. 2(a). From the images, the surface normal for each facet is determined

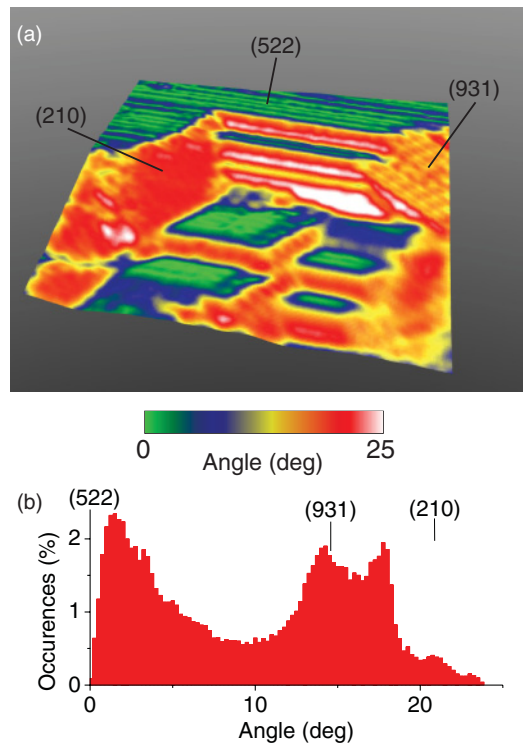


FIG. 4. (Color) (a) Same topography as shown in Fig. 2(a) overlaid with a colored map, where the color encodes the local angle relative to a (522) facet. The pseudo-3D projection shows the surface with isotropic scale (lateral and vertical dimensions are scaled by the same factor). (b) Histogram of the image in (a) showing peaks at the angles at which a facet is seen in the topography, black vertical lines indicate the expected angles (see also Table I for a direct comparison). There is a systematic deviation between expected and measured angles which increases with increasing angle, which is likely due to uncertainty in the piezocalibration and drift.

TABLE I. Angles of various facets with respect to the (522) facet. The error bars are determined as the standard deviation of the average taken over an extended area on each facet.

Facet	Calculated	Measured
(210)	20.9	$17.9 \pm 0.3$
(611)	16.2	$15.9 \pm 2.8$
(931)	14.7	$14.3 \pm 0.8$

and the angles are calculated. If the main crystallographic directions with respect to the orientation of the topographic image are known, the Miller indices of neighboring facets can be determined (the methods are not completely independent, as for the second one at least one facet has to be determined from the surface atomic structure). Figure 4(a) shows the resulting map of angles with respect to a specific facet, here a (522) facet. This procedure could be applied to all facets except the (110) facet, which we did not observe in the same field of view as the other facets. The measured angles between different facets are shown in comparison to the angles calculated from the Miller indices in Table I [see also the histogram in Fig. 4(b)]. The crystallographic structure of the most important other alloy formed by ytterbium and aluminum,<sup>25</sup> YbAl<sub>2</sub>, differs from that of YbAl<sub>3</sub><sup>12</sup> and can be expected to expose significantly different surface structures.

### C. Tunneling Spectroscopy

Figure 5(a) shows a tunneling spectrum acquired on a (110) facet. Besides a peak close to the Fermi energy (marked as K), two satellite peaks at +1.2 eV and -1.2 eV (marked as SO1 and SO2) are found. A similar satellite attributed to spin-orbit splitting is observed in the occupied states by photoemission at -1.2 eV.<sup>19</sup> In addition, a broad maximum (labeled S) around -0.5 eV is seen whose intensity varies strongly depending on the position on the (110) facet where the spectrum is taken; it likely originates from the reconstructed surface layer of the (110) facet. In Fig. 5(b), tunneling spectra are shown for the facets investigated. In each case, at least one peak can be found in the range between -100 mV and the Fermi energy, in many cases a double peak structure [with the exception of the (110) facet]. Spectra acquired in a narrower energy range close to the Fermi energy are shown in Fig. 6(a). The intensities of the peaks depend on the exact position within the facet where the spectra are acquired. This is shown exemplarily in Fig. 6(b) for the (210) facet; both the relative and absolute intensities of the two peaks change considerably depending on whether

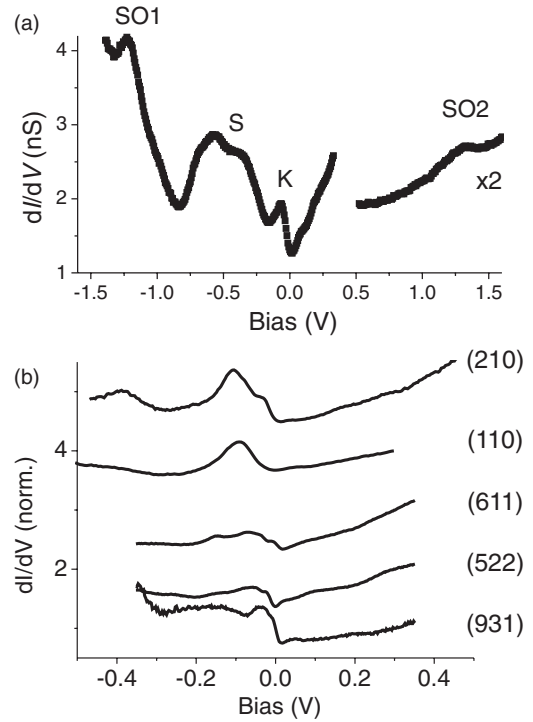


FIG. 5. (a) Overview tunneling spectrum acquired on a (110) facet at 77 K, the spectrum is composed of two spectra taken with different stabilization conditions before switching off the feedback loop ( $V = 0.4$  V,  $I = 0.8$  nA;  $V = 2.546$  V,  $I = 3$  nA) (Ref. 26). Besides a peak close to the Fermi energy (marked as K), a broad maximum around -0.5 V (marked as S) and two satellites (SO1 and SO2) can be seen. (b) STS on different crystallographic facets of YbAl<sub>3</sub>; spectra are acquired at 6 K except for the (110) facet (77 K). Spectra are shifted vertically for clarity.

spectra are taken at a position on the surface imaged higher compared to one which is imaged lower.

Peak positions and widths have been extracted by fitting Fano line shapes to the peaks, which is an established procedure to evaluate the Kondo effect of adatoms studied by STS.<sup>27,28</sup> Recently, it has been shown that the tunneling spectra of a Kondo lattice in the vicinity of the Fermi energy can also be described by a Fano resonance.<sup>1,2,6</sup> We have determined the peak positions and widths as listed in Table II by fitting Fano functions of the form

$$\frac{dI}{dV} = \sum_{i=1\dots n} a_i \frac{(q_i + \tilde{\epsilon}_i)^2}{1 + \tilde{\epsilon}_i^2} + c, \quad (2)$$

TABLE II. Peak positions  $\epsilon_n$  and widths  $\Delta_n$  determined from STS spectra. The index 1 refers to the peak closer to the Fermi energy (except for (611), where an additional peak is found right at the Fermi energy). The overall average has been taken over the 6.7 K measurements.

Facet	$T$ [K]	$\epsilon_1$ [mV]	$\Delta_1$ [mV]	$\epsilon_2$ [mV]	$\Delta_2$ [mV]
(210)	6.7	$-28.4 \pm 3.8$	$24.9 \pm 8.1$	$-102 \pm 7$	$44.3 \pm 9.7$
(110)	77	-	-	$-76.9 \pm 17.3$	$54.3 \pm 16$
(611)	6.7	$-31.2 \pm 0.6$	$18.5 \pm 0.9$	-	-
(522)	6.7	$-19.1 \pm 0.9$	$5.6 \pm 0.7$	-	-
(931)	6.7	$-25.6 \pm 6.6$	$29.3 \pm 8.9$	-	-
Average	6.7	$-25.7 \pm 5.0$	$19.9 \pm 10.6$	-	-

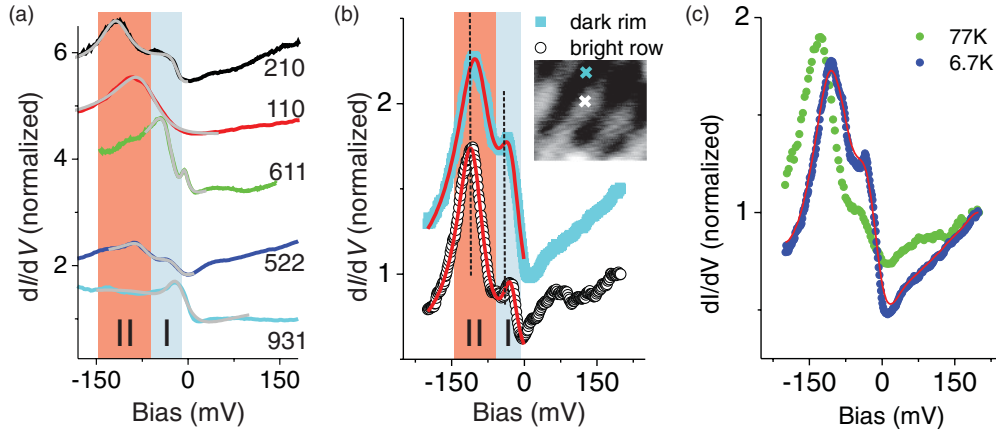


FIG. 6. (Color) (a) STS on different crystallographic facets of YbAl<sub>3</sub> close to the Fermi energy, spectra are acquired at 6.7 K except for the (110) facet (77 K); the shaded regions tentatively assign the resonances to bulk (I) and surface (II) related features [solid lines show fits of Eq. (2)]. (b) Spectra on a (210) facet taken at 6.7 K in different locations on the surface. The red solid lines show fits of the sum of two Fano functions to the 6 K spectra to extract the peak positions and widths. Vertical lines are shown as a guide to the eye to allow for a comparison of the peak positions. Shading of regions as in (a), spectra in (a) and (b) are shifted vertically for clarity. Inset in (b) shows the two positions where the spectra have been taken on the (210) facet. (c) Temperature dependence of spectra on the (210) facet; shown are a spectrum acquired at 6.7 K and at 77 K. In addition, shown as a solid red line, the 6.7 K spectrum is broadened as if it would have been taken at 77 K by accounting for the broadening of the Fermi distribution. The comparison shows that the changes in spectra cannot be explained due to only the temperature broadening.

where  $\tilde{\epsilon}_i = \frac{\omega - \epsilon_{K_i}}{\Delta_i}$  and  $\omega = eV$ , and  $n$  is the number of resonances observed in the energy range which is considered. Each resonance is described by four parameters:  $a_i$  is related to the amplitude of the resonance,  $q_i$  to the line shape (ranging from  $q_i = 0$  describing a dip via an asymmetric line shape for  $q_i = 1$  to a peak for  $q_i \rightarrow \infty$ ),  $\epsilon_{K_i}$  to its position, and  $\Delta_i$  to its half width. Thus, in cases where the spectra show two resonances, nine parameters were fitted, the eight related to the two resonances plus another one to account for a constant background. We note that in many spectra, the resonances appear to have a fine structure which, however, is not clearly and reproducibly resolved in our spectra. The resulting parameters for both peaks are summarized in Table II. While a systematic study of the temperature dependence of the spectra is beyond the scope of this paper, Fig. 6(c) shows spectra acquired at 6.7 K and at 77 K on a (210) facet. Whereas the peak at  $-100$  mV preserves its intensity and shape, we find a significant decrease in the peak height of the peak at  $-30$  mV. This behavior can clearly not be understood just by thermal broadening. To stress this point, a simulated spectrum is shown in Fig. 6(c) which is obtained by broadening the spectrum acquired at 6.7 K by the thermal smearing expected at 77 K.

#### IV. DISCUSSION

From the atomic scale analysis of topographic images of our YbAl<sub>3</sub> crystals, we see a reconstruction of the surface. Accordingly, through the investigation of the surface dependence of our tunneling spectra, we identify two energy scales. We observe a peak between  $-70$  mV and the Fermi energy on all facets except (110) [marked as regime I in Fig. 6(a)]. By comparison with the expected energy of the bulk Kondo resonance and from the comparatively small sensitivity of this

resonance on the position on the facet or its orientation, we attribute it to bulk properties of the crystal. The remaining dependence on the orientation of the facet could be due to preferential tunneling to states with small  $k_{||}$ , an anisotropic band structure or a non-negligible influence of the surface in an extended surface region.

We attribute the strong additional resonance found on (110) and (210) facets at lower energies to the influence of the surface. YbAl<sub>3</sub> is known from photoemission measurements to become divalent at the surface, with the divalent layer having a thickness of  $\sim 5$  Å.<sup>9,10</sup> Thus a bulk feature has to be probed through this surface layer. A divalence of ytterbium at the surface is also consistent with the reconstruction of the surface layer which we find on low index facets. Divalent ytterbium in bulk compounds has an ionic radius which is more than 15% larger than that of trivalent ytterbium.<sup>29</sup> Thus on facets which expose close-packed rows of ytterbium, a reconstruction of these rows can be expected. Of the facets we have investigated, this is the case for (110) and (210). For completely divalent ytterbium, no Kondo resonance is expected. Similarly, no surface states have been reported at the surface of ytterbium compounds in the vicinity of the Fermi energy.<sup>9,10,19</sup> Crystal field splitting, which if sufficiently large can lead to a split Kondo resonance, could lead to multiple resonances close to the Fermi energy. If there is significant crystal field splitting in YbAl<sub>3</sub>, it is expected to be below 10 mV,<sup>30</sup> significantly lower than what would be required to explain the second peak. The resonance could be explained by ytterbium close to the surface not being rendered completely divalent, but somewhere between di- and trivalent with a valence lower than the bulk value. With reduced valence, the Kondo resonance moves away from the Fermi energy until eventually the  $f$  shell is completely filled and there is no Kondo resonance anymore. We note that on (522) and (611) facets, we do also see some

weak additional structure in the range from  $-50$  to  $-200$  mV, which however is much weaker and less well defined than the ones we observe on the (210) and (110) facets.

In order to connect our results to macroscopic bulk data of  $\text{YbAl}_3$ , we have determined an average position of the bulk-related peak by taking into account all facets investigated with equal weight. This procedure can be expected to give only a rough estimate for the Kondo scale because the selection of facets is random. The resulting position and width of the resonance are summarized in Table II. We obtain an average energy position of  $-25.7 \pm 5.0$  mV (corresponding to a Kondo temperature of  $298 \pm 58$  K, cf. Refs. 19 and 31). This is roughly consistent with the Kondo temperature estimated from the magnetic susceptibility measurements. Position and width of the Kondo resonance extracted from the zero-temperature limit of the magnetization and the linear coefficient of the specific heat at low temperature yields a position of  $-42.7$  mV and a width of  $17.7$  mV.<sup>31</sup>

Our results for the bulk-related resonance are in reasonable agreement with photoemission data<sup>17,19,32</sup> taking into account that photoemission averages over all exposed crystallographic facets. In photoemission, a peak around 35 meV below the Fermi energy (at 10 K) with a full width of 50 meV has been identified as a signature of the Kondo effect.<sup>17</sup> The variation of the electronic structure we find for the various facets of  $\text{YbAl}_3$  might explain the differences in photoemission spectra of  $\text{YbAl}_3$  as measured by various groups<sup>17-19</sup> and also compared to our measurements.

SQUID measurements show an additional low temperature scale associated with the maximum in the magnetization at 14 K. This maximum in the magnetization has been

connected to the formation of a pseudogap<sup>33</sup> observed in optical conductivity measurements.<sup>34</sup> We observe an additional low energy peak right at the Fermi energy with a width of  $7.8 \pm 0.4$  mV [see Fig. 6(a) spectra for (611) facets] on some of the facets, which possibly corresponds to the formation of this pseudogap and the low energy scale in  $\text{YbAl}_3$ .

## V. CONCLUSIONS

We have studied the surface of a rare earth compound by STM. Topographic imaging of multiple facets allowed us to identify the different facets of  $\text{YbAl}_3$  and investigate the surface dependence of tunneling spectra. Thereby we could analyze the tunneling spectra in terms of features whose energy is consistent with bulk properties and others which are likely surface related, due to a change in the valence of near-surface ytterbium. Exploiting the valence change of ytterbium ions in the surface region might allow us to investigate electron correlations in 2D systems, where they can be expected to be more important than in 3D systems. The preparation of such a 2D Kondo lattice has been demonstrated recently for thin films prepared by molecular beam epitaxy.<sup>3</sup> Electronic correlations have been found to be substantially enhanced by the reduced dimensionality.

## ACKNOWLEDGMENTS

We acknowledge C. Busch for technical assistance in growing  $\text{YbAl}_3$  crystals and V. Duppel for SEM and EDAX characterization of  $\text{YbAl}_3$  samples.

\*Present address: Institut for Fysik og Nanoteknologi and Interdisciplinary Nanoscience Center (iNANO), Aalborg Universitet, Skjernvej 4A, DK-9220 Aalborg, Denmark.

†Present address: Lehrstuhl für Festkörperphysik, Universität Erlangen-Nürnberg, Staudtstraße 7, D-91058 Erlangen, Germany.

‡Present address: Carl Zeiss SMT AG, D-73446 Oberkochen, Germany.

<sup>1</sup>M. Maltseva, M. Dzero, and P. Coleman, *Phys. Rev. Lett.* **103**, 206402 (2009).

<sup>2</sup>K. Haule and G. Kotliar, *Nat. Phys.* **5**, 796 (2009).

<sup>3</sup>H. Shishido, T. Shibauchi, K. Yasu, T. Kato, H. Kontani, T. Terashima, and Y. Matsuda, *Science* **327**, 980 (2010).

<sup>4</sup>D. Hsieh, D. Qian, L. Wray, Y. Xia, Y. S. Hor, R. J. Cava, and M. Z. Hasan, *Nature (London)* **452**, 970 (2008).

<sup>5</sup>D. V. Vyalikh, S. Danzenbächer, Yu. Kucherenko, C. Krellner, C. Geibel, C. Laubschat, M. Shi, L. Patthey, R. Follath, and S. L. Molodtsov, *Phys. Rev. Lett.* **103**, 137601 (2009).

<sup>6</sup>A. R. Schmidt, M. H. Hamidian, P. Wahl, F. Meier, A. V. Balatsky, J. D. Garrett, T. J. Williams, G. M. Luke, and J. C. Davis, *Nature (London)* **465**, 570 (2010).

<sup>7</sup>P. Aynajian, E. H. da Silva Neto, C. V. Parker, Y. Huang, A. Pasupathy, J. Mydosh, and A. Yazdani, *Proc. Nat. Ac. Sci.* **107**, 10383 (2010).

<sup>8</sup>D. Ehm, S. Hufner, F. Reinert, J. Kroha, P. Wölfe, O. Stockert, C. Geibel, and H.v. Löhneysen, *Phys. Rev. B* **76**, 045117 (2007).

<sup>9</sup>G. Kaindl, B. Reihl, D. E. Eastman, R. A. Pollak, N. Mårtensson, B. Barbara, T. Penney, and T. S. Plaskett, *Solid State Commun.* **41**, 157 (1982).

<sup>10</sup>R. Fasel, P. Aebi, J. Osterwalder, and L. Schlapbach, *Surf. Sci.* **394**, 129 (1997).

<sup>11</sup>S. Ernst, S. Kirchner, C. Krellner, C. Geibel, G. Zwicknagl, F. Steglich, and S. Wirth, *Nature (London)* **474**, 362 (2011).

<sup>12</sup>E. E. Havinga, K. H. J. Buschow, and H. J. van Daal, *Solid State Commun.* **13**, 621 (1973).

<sup>13</sup>A. L. Cornelius, J. M. Lawrence, T. Ebihara, P. S. Riseborough, C. H. Booth, M. F. Hundley, P. G. Pagliuso, J. L. Sarrao, J. D. Thompson, M. H. Jung, A. H. Lacerda, and G. H. Kwei, *Phys. Rev. Lett.* **88**, 117201 (2002).

<sup>14</sup>T. Ebihara, E. D. Bauer, A. L. Cornelius, J. M. Lawrence, N. Harrison, J. D. Thompson, J. L. Sarrao, M. F. Hundley, and S. Uji, *Phys. Rev. Lett.* **90**, 166404 (2003).

<sup>15</sup>E. D. Bauer, C. H. Booth, J. M. Lawrence, M. F. Hundley, J. L. Sarrao, J. D. Thompson, P. S. Riseborough, and T. Ebihara, *Phys. Rev. B* **69**, 125102 (2004).

<sup>16</sup>J. C. P. Klaasse, F. R. de Boer, and P. F. de Châtel, *Physica B* **106**, 178 (1981).

<sup>17</sup>L. H. Tjeng, S.-J. Oh, E.-J. Cho, H.-J. Lin, C. T. Chen, G.-H. Gweon, J.-H. Park, J. W. Allen, T. Suzuki, M. S. Makivić, and D. L. Cox, *Phys. Rev. Lett.* **71**, 1419 (1993).

<sup>18</sup>F. Patthey, J.-M. Imer, W.-D. Schneider, Y. Baer, B. Delley, and F. Hulliger, *Phys. Rev. B* **36**, 7697 (1987).

- <sup>19</sup>S.-J. Oh, S. Suga, A. Kakizaki, M. Taniguchi, T. Ishii, J.-S. Kang, J. W. Allen, O. Gunnarsson, N. E. Christensen, A. Fujimori, T. Suzuki, T. Kasuya, T. Miyahara, H. Kato, K. Schönhammer, M. S. Torikachvili, and M. B. Maple, *Phys. Rev. B* **37**, 2861 (1988).
- <sup>20</sup>R. I. R. Blyth, J. J. Joyce, A. J. Arko, P. C. Canfield, A. B. Andrews, Z. Fisk, J. D. Thompson, R. J. Bartlett, P. Riseborough, J. Tang, and J. M. Lawrence, *Phys. Rev. B* **48**, 9497 (1993).
- <sup>21</sup>A. Hiess, J. X. Boucherle, F. Givord, and P. C. Canfield, *J. Alloys Compd.* **224**, 33 (1995).
- <sup>22</sup>A. Hiess, J. X. Boucherle, F. Givord, J. Schweizer, E. Lelièvre-Berna, F. Tasset, B. Gillon, and P. C. Canfield, *J. Phys. Condens. Matter* **12**, 829 (2000).
- <sup>23</sup>O. Gunnarsson and K. Schönhammer, *Phys. Rev. B* **28**, 4315 (1983).
- <sup>24</sup>J. J. Joyce, A. B. Andrews, A. J. Arko, R. J. Bartlett, R. I. R. Blyth, C. G. Olson, P. J. Benning, P. C. Canfield, and D. M. Poirier, *Phys. Rev. B* **54**, 17515 (1996).
- <sup>25</sup>T. B. Massalski, *Binary Alloy Phase Diagrams*, Vol. 1 (American Society for Metals, Ohio, 1986).
- <sup>26</sup>The spectrum has been acquired in two parts out of technical reasons: (1) because the software did not allow for more than 256 points for a spectrum, (2) the tunneling setpoint and the settings for the lock-in amplifier were optimized for the respective ranges.
- <sup>27</sup>J. Li, W. D. Schneider, R. Berndt, and B. Delley, *Phys. Rev. Lett.* **80**, 2893 (1998).
- <sup>28</sup>V. Madhavan, W. Chen, T. Jamneala, M. F. Crommie, and N. S. Wingreen, *Science* **280**, 567 (1998).
- <sup>29</sup>A. Iandelli, in *Rare Earth Research*, edited by E. V. Kleber (MacMillan, New York, 1961), p. 135.
- <sup>30</sup>U. Walter, E. Holland-Moritz, and Z. Fisk, *Phys. Rev. B* **43**, 320 (1991).
- <sup>31</sup>D. M. Newns and N. Read, *Adv. Phys.* **36**, 799 (1987).
- <sup>32</sup>E.-J. Cho, S.-J. Oh, C. G. Olson, J.-S. Kang, R. O. Anderson, L. Z. Liu, J. H. Park, and J. W. Allen, *Physica B* **186-188**, 70 (1993).
- <sup>33</sup>The expression pseudogap is meant here to imply only that the density of states inside the gap is not completely suppressed.
- <sup>34</sup>H. Okamura, T. Michizawa, T. Nanba, and T. Ebihara, *J. Phys. Soc. Jpn.* **73**, 2045 (2004).